Elastomers and Composites
Vol. 61, No. 1, pp. 1~7 (March 2026)

Print ISSN 2092-9676/Online ISSN 2288-7725
DOI: https://doi.org/10.7473/EC.2026.61.1.1

Morphology-Directed Growth of Urchin-like Au Nanoparticles Using Modular Microfluidic Chips

Hayoung Kim[*,,‡], Jaejun Park[*,**,‡], and Seunghyun Lee[*,**,***,†]**

[*]*Department of Applied Chemistry, Hanyang University ERICA, Ansan 15588, Republic of Korea*
[**]*Center for Bionano Intelligence Education and Research, Hanyang University ERICA, Ansan 15588, Republic of Korea*
[***]*Department of Energy and Bio Sciences, Hanyang University ERICA, Ansan 15588, Republic of Korea*

(Received October 31, 2025, Revised March 30, 2026, Accepted March 31, 2026)

Abstract: A modular microfluidic platform was used to continuously synthesize urchin-like Au nanoparticles (Au NPs). In contrast to conventional methods, the particles synthesized via this flow chemistry have protruding surfaces that make the formation of hot spots in plasmonic. The microfluidic platform enables the continuous synthesis of Au NPs with reproducibility and uniformity within a short reaction time. The optical properties of the Au NPs were characterized using UV-VIS spectroscopy, and particle size and distribution were evaluated by dynamic light scattering (DLS). Scanning electron microscopy (SEM) was used to confirm the surface morphology and size of the Au NPs. Raman spectroscopy shows surface enhanced Raman scattering (SERS) which enhancement factor (EF) was 4.01×10^6. These results suggest that this microfluidic synthesis approach can be applied to fabricate of morphologically controlled metal nanoparticles that can be able to applicable to optical sensors.

Keywords: flow chemistry, plasmonic nanoparticle, lab on a chip, LSPR, SERS

Introduction

Nanoparticles are actively researched across diverse fields due to their unique properties, characterized by sizes ranging from a few to hundreds of nanometers. Nanoparticles exhibit high specific surface area, quantum size effects, and specific physical and chemical properties that manifest depending on their composition and structure, granting them broad application potential in various areas such as electrochemical catalysts, optical sensors and etc.[1-7] In particular, precise control of the structure that includes size, shape, and surface properties is considered a key factor determining their functional performance and applicability. Surface modification and structural control enable their utilization in various applications.[8,9] Accordingly, a growing number of researchers aim to effectively and reproducibly synthesize nanoparticles for application in such as optical sensors, catalysts by use diverse precursors, synthesis routes, and reaction conditions.[10,11]

Among these nanoparticles, plasmonic nanoparticles exhibit unique optical behavior due to their localized surface plasmon resonance (LSPR) phenomenon. LSPR arises from the interaction between incident light and the collective free electrons on the surface of metallic nanoparticles, known as plasmons. Au NPs, in particular, are widely used in various optical and life science applications due to their chemical stability and biocompatibility.[12-17] The optical properties of these gold nanoparticles can be sensitively tuned by the nanoparticle size, composition, and surface morphology.[18-21]

To optimize the performance of these plasmonic nanoparticles, control over their size and surface morphology is essential. Microfluidic platforms are gaining attention as an innovative synthesis platform to address this challenge. Microfluidic platforms are continuous flow-based synthesis platforms capable of precisely regulating fluid flow, mixing, temperature, and reaction time. In particular, modular microfluidic platforms can sequentially integrate various reaction steps, providing process flexibility and controllability. This enables not only effective control of nanoparticle surface morphology and size but also rapid optimization of reaction conditions.[22-24]

[†]Corresponding author E-mail: leeshyun@hanyang.ac.kr
[‡]These authors contributed equally to this work.

Recent studies recognize that controlling nanoparticle surface roughness and complex shapes are key factors in enhancing plasmonic performance. The greater the number of protrusions or similar structures on the surface, the more hot spots form on the particle surface, maximizing the electric field enhancement. This enables the detection of trace molecules in SERS-based detection. This control of fine surface structures plays a pivotal role in high-sensitivity molecular detection fields such as LSPR-based sensors and SERS-based sensors. For example, Au NPs with uniformly controlled surfaces can effectively detect even minor changes in biomolecules bound to their surfaces, enabling the detection of trace target molecules in SERS-based detection.[25-35]

Given the importance of surface morphology control, numerous studies have focused on enhancing sensor performance by tuning the optical properties of nanoparticles through controlling the surface morphology.[36-39] Therefore, in this study, we aimed to achieve the continuous synthesis of uniform urchin-like Au NPs by applying previously reported shape control methods within a modular microfluidic system.[39] This flow-based synthesis approach overcomes the lack of reproducibility and size control limitations of conventional methods, providing plasmonic nanoparticles with excellent optical properties through continuous and stable synthesis conditions. By evaluating the SERS performance of the synthesized Au NPs, we demonstrate the practical feasibility of this plasmonic platform for molecular detection.

Experimental

1. Materials

Gold (III) chloride trihydrate ($HAuCl_4$, ≥99.9%), L-ascorbic acid (99%), and Gum Arabic from acacia tree were purchased from Sigma-Aldrich. The gold (III) chloride solution was used as a 25 mM stock solution.

2. Fabrication of Urchin-like Au nanoparticles

Urchin-like Au NPs were synthesized using a flow chemistry approach. The synthetic procedure was adapted from the meat ball-like Au NPs synthesis protocol reported by Wang et al.[39] While maintaining the same precursors as described in the original method, the experimental conditions were modified to accommodate the microfluidic system follows: Solution A was prepared by mixing 20 mL of 25 mM $HAuCl_4 \cdot 3H_2O$ with 5 mL of 1 wt% gum arabic solution, resulting in 25 mL of 20 mM $HAuCl_4 \cdot 3H_2O$ containing 0.2 wt% gum arabic. Solution B was prepared by dissolving L-ascorbic acid (100 mM) and 0.05 g of gum arabic in DI water to obtain a final volume of 25 mL with 0.2 wt% gum arabic. Solutions A and B were introduced into the microfluidic device through Inlet 1 and Inlet 2, respectively, using syringe pumps. To quench the reaction, DI water was introduced through Inlet 3. (See Fig. 1)

3. Characterization

Ultraviolet-visible-near-infrared absorption spectra were obtained using a JASCO V-770 spectrophotometer. Morphological features were investigated using field-emission scanning electron microscopy (FE-SEM) (HITACHI-S4800) at an accelerating voltage of 15.0 kV. Raman spectra images were acquired using confocal micro-Raman spectroscopy with a dark-field microscope (WEVE, HEDA). The following excitation sources were used: a 785 nm single longitudinal mode DPSS laser (130 mW); (Integrated Optics). Raman scattering signals were collected using a charge-coupled device camera with a high-resolution grating (1200 grooves mm^{-1}) and measured by focusing a laser spot using a 100 × (NA 0.9) objective lens with a diffraction limit of ≈ 200 nm.

Results and Discussion

Figures 1 and 2 describe the continuous-flow setup built on a modular microfluidic chip for Au NP synthesis. A pressure pump coupled with a flow sensor enabled precise adjustment of flow rates under varying experimental conditions. In the Y-shaped module, Solution A and Solution B are injected into separate channels, converge into a single channel, and then enter the curved mixing module. This module employs a passive mixing structure. As shown in Figure 2, the two solutions initially maintain a laminar flow state. Gradually, uniform mixing occurs due to Dean flow in the curved section and molecular diffusion. At this point, color changes during the laminar flow and mixing processes were visually observed. After mixing was complete, DI water was injected via the T-shaped module to quench and dilute the product. This continuous process yielded uniform urchin-like Au NPs, with morphology tunable by adjusting the flow rates of Solutions A and B. The synthesized AU NPs' morphology, size distribution, and optical properties were characterized

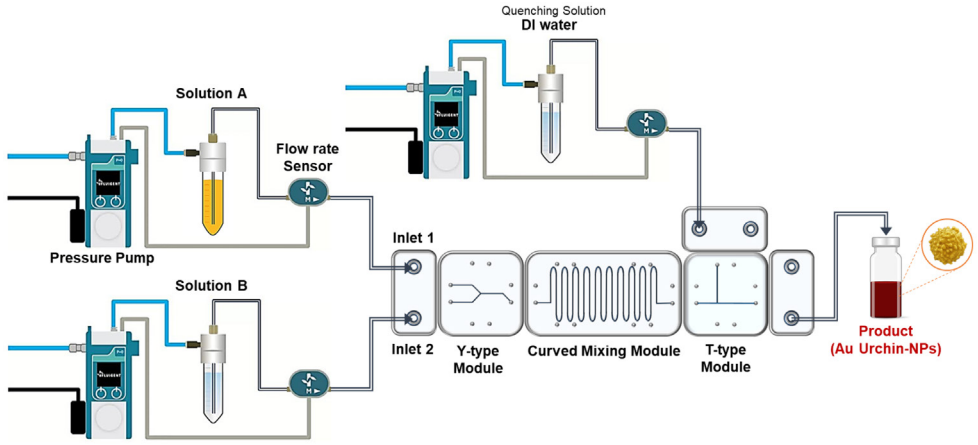

Figure 1. Schematic diagram of the modular microfluidic system.

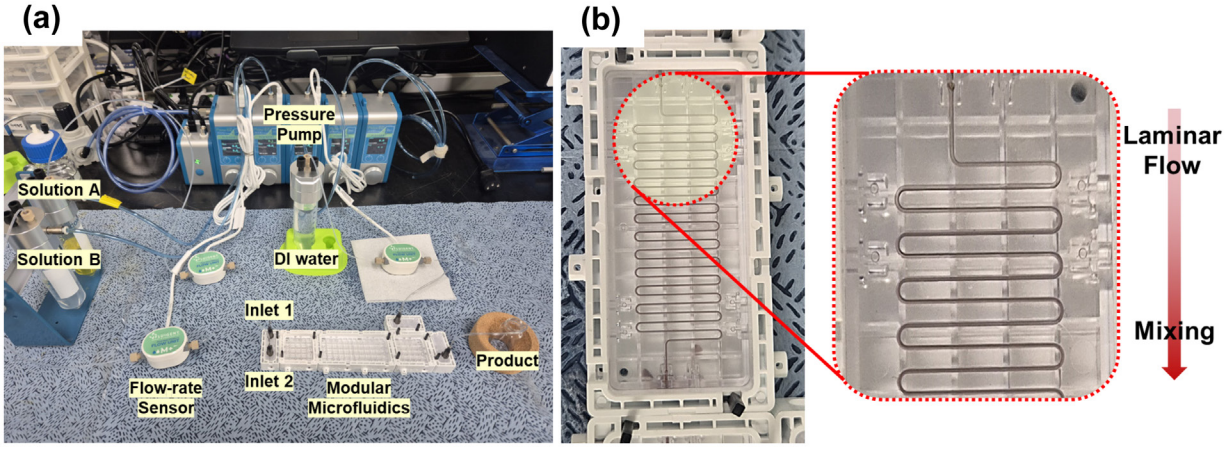

Figure 2. (a) Photograph of the actual modular microfluidic system setup used for nanoparticle synthesis. (b) Visualization of the transition from laminar flow to a mixed state within the curved mixing module of the modular microfluidic chip.

by SEM, DLS, UV-Visible spectroscopy, and Raman spectroscopy.

Both Urchin-like Au NPs and Au Meatball-like NPs were synthesized using the same reagent, yet distinct differences emerged in the optical properties of the particles obtained by each method. Particle sizes were determined by UV-Visible

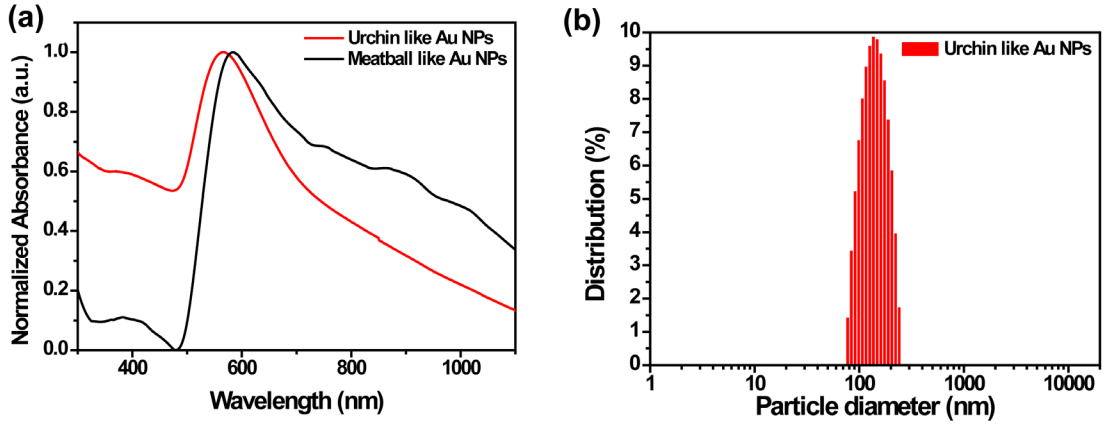

Figure 3. (a) Urchin-like Au NPs and Meatball-like Au NPs' Normalized UV-Visible spectrum (b) DLS spectrum of Au nanoparticle which is synthesized by Microfluidic chip.

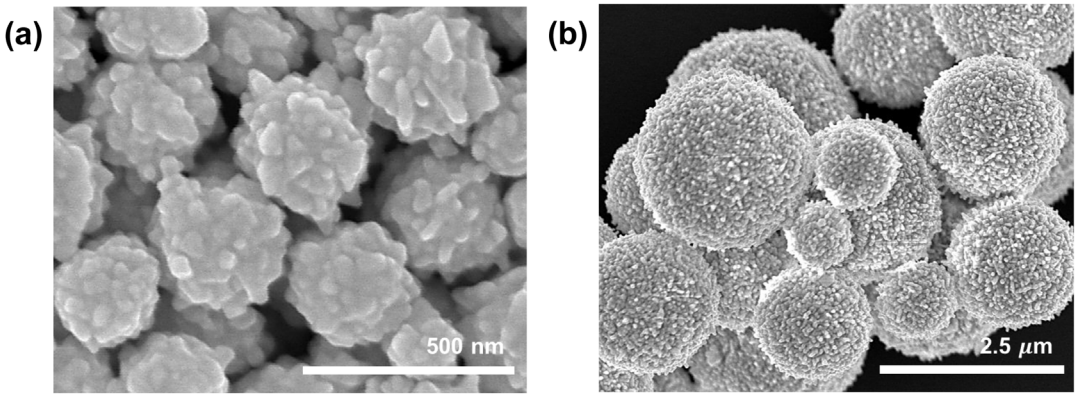

Figure 4. (a) SEM image of Urchin-like Au NPs by using microfluidic chips (Scale bar = 500 nm) and (b) SEM image of Meat ball-like Au NPs (Scale bar = 2.5 μm).

spectroscopy and DLS. Figure 3(a) shows the normalized UV–Visible spectra of both samples. The urchin-like Au NPs exhibit a narrower peak width at half-maximum, whereas the Meatball-like Au NPs show a broader peak with additional shoulder around 800 nm. These results indicate that microfluidic synthesis affords superior uniformity and optical stability compared to the conventional method. DLS results in Figure 3(b) reveal a mean of particle diameter of 259.167±9.66 nm with a size variation of 3.73%.

Figure 4 SEM images clearly confirm both the uniformity of the particle size distribution and the distinctive urchin-like Au NPs synthesized using modular microfluidic chips. This shows that the particle shape-controlled synthesis method utilizing a modular microfluidic system provides high precision in terms of nanoparticle size control and quality assurance.

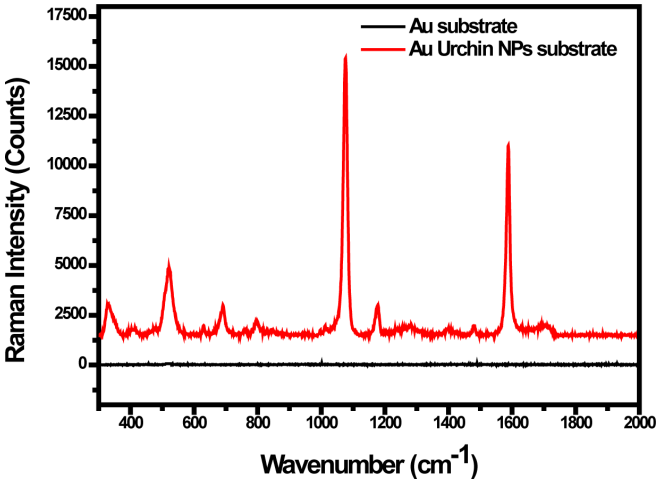

Figure 5. Urchin-like Au NPs on flat Au substrate and flat Au substrate's Raman spectrum with 4-mercaptobenzoic acid.

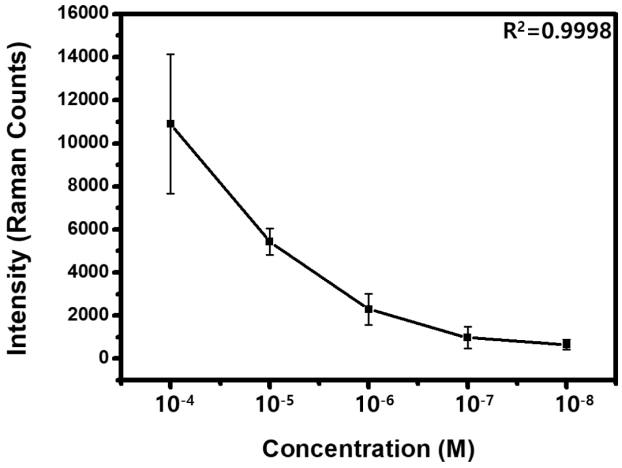

Figure 6. SERS signal by concentration of 4-mercaptobenzoic acid. Each Raman measurement was taken five times at random points.

We measured Raman spectroscopy on substrate which use urchin-like Au NPs for molecular detection. Spectra were acquired with exposure times of 1 s for verifying the performance of the SERS with a laser power of 0.45 mW after applying a 1% neutral density filter. For the background subtraction, the mean difference equation was calculated using a window size of 15. Through following calculations, we were able to derive the following enhancement factor, and by measuring concentrations using SERS-active substrates with Urchin-like Au NPs, we confirmed that measurements are possible down to 10^{-8} M. (See Figure 6).

The enhancement factor (EF) in our study was calculated as following equation[30-32]:

$$\text{Enhancement factor (EF)} = (I_{SERS} / N_{SERS}) / (I_{REF} / N_{REF})$$

I_{SERS} = 13945.4, I_{REF} = 10.12 (in Figure 5)

N_{SERS} = number of Raman Tag molecules

N_{REF} = calculated by estimating the number of molecules in the confocal volume of a cylinder with a diffraction-limited spot by considering the molecular weight and density of Raman tag molecule (4-Mercaptobenzoic acid). The density of Raman tag, taken from literature was 9.85×10^6.[40]

$$N_{REF} = \frac{Density \cdot V_{laser} \cdot N_A}{M}$$

(V_{laser}: laser's confocal volume, N_A: Avogadro number, M: molecule weight[g/mol])

$$V_{laser} = Focal\ Volume = \pi r^2 h$$

$$r = Focal\ Radius = \frac{0.61\lambda}{NA}$$

$$h = Focal\ Depth = \frac{2n\lambda}{NA^2}$$

$$\therefore\ N_{REF} = 1.04\times10^{10}$$

N_{SERS} = (Measured Area)/(Minimum area required for molecular adsorption)

Surface of Measured Area = pi × r^2 = $(5.32\times10^{-5}\ cm)^2$ = $8.89\times10^{-9}\ cm^2$

$N_{SERS} = 8.89\times10^{-9}\ cm^2 / 2.5\times10^{-15}\ cm^2 = 3.56\times10^6$

$$\therefore\ \text{Enhancement Factor} = \frac{13945.4}{3.56\times10^6} \Big/ \frac{10.13}{9.06\times10^9} = 4.01\times10^6$$

This EF presents the probability to use the urchin-like Au NPs for optical sensors such as biosensor, molecular detections and etc.[41-44]

Conclusions

In this study, urchin-like Au NPs were synthesized with well dispersed and uniformed using a modular microfluidic chip. Beyond simple spherical particles, a new form of nanoparticle with a unique surface structure can be formed in a single-step process were confirmed. Furthermore, Evaluation of the SERS performance of the synthesized nanoparticles revealed a distinct signal enhancement effect to use optical sensing. This research is expected to enable the synthesis of nanoparticles with diverse structures based on a modular microfluidic platform, allowing control not only over particle size but also surface morphology. Using diverse metal precursors, it will be possible to develop novel nanoparticle shapes or structures that differ from existing ones. These developed particles can be utilized in optical sensors, biosensors, and molecular detection sensors, similar to previously reported studies. This research presents potential applications for SERS-based biosensors by applying them to substrates with diverse structures.

Acknowledgements

This work was supported by grants from the Technology Innovation Program (20022507) funded By the Ministry of Trade, Industry & Energy (MOTIE, Korea), and the GRRC program of Gyeonggi Province (GRRCHanyang2020-B03).

Conflict of Interest: The authors declare that there is no conflict of interest.

References

1. T. H. Kim, H. Kim, H. J. Jang, N. Lee, K. H. Nam, D. Chung, and S. Lee, "Improvement of the thermal stability of dendritic silver-coated copper microparticles by surface modification based on molecular self-assembly", *Nano Converg.*, **8**, 15 (2021).
2. T. H. Kim, D. C. Cha, J. C. Jeong, and S. Lee, "Facile fabrication of carbon nanotubes@CuO composites by microwave method", *Elast. Compos.*, **56**, 113 (2021).
3. C. Y. Lee, T. H. Kim, J. Park, W. S. Yang, and S. Lee, "Morphology-controlled mesoporous core–shell carbon nanospheres decorated with Cu nanoparticles as highly efficient and reusable catalyst", *Mater. Today Chem.*, **42**, 102433 (2024).
4. H. Naseer, M. Jeon, H. Kim, and J. H. Bang, "Impact of interfacial binding between Au nanoclusters and TiO_2 on solar cell performance", *Surf. Interfaces*, 106827 (2025).
5. M. A. Abbas, M. Jeon, and J. H. Bang, "Understanding the photoelectrochemical behavior of metal nanoclusters: a perspective", *J. Phys. Chem. C*, **126**, 16928 (2022).
6. M. Jeon, H. Kim, S. Yoo, S. Park, G. Leem, S. Lee, and J. H. Bang, "Unveiling the critical role of crystallinity in photogenerated hole transfer behavior of TiO_2 with an aminoxyl radical mediator", *J. Ind. Eng. Chem.*, **140**, 190 (2024).
7. M. Shin, W. Kim, K. Yoo, H. S. Cho, S. Jang, H. J. Bae, J. An, J. Lee, H. Chang, D. E. Kim, J. Kim, Luke P. Lee, and B. H. Jun, "Highly sensitive multiplexed colorimetric lateral flow immunoassay by plasmon-controlled metal–silica isoform nanocomposites: PINs", *Nano Converg.*, **11**,

42 (2024).
8. W. Kim, G. Ryu, K. Hwang, S. Song, and W. Kim, "Effect of coagulant type on the silica dispersion and properties of functionalized RAFT ESBR silica wet masterbatch", *Elast. Compos*., **55**, 167 (2020).
9. S. H. Hong and S. H. Hwang, "A concise review of recent application progress and future prospects for lignin as biomass utilization", *Elast. Compos*., **56**, 136 (2021).
10. S. Yoo, D. H. Nam, T. I. Singh, G. Leem, and S. Lee, "Effect of reducing agents on the synthesis of anisotropic gold nanoparticles", *Nano Converg.*, **9**, 5 (2022).
11. S. Yoo, G. Youn, H. Lee, J. S. Kwon, Y. Lee, and S. Lee, "Synthesis of ultra-small gold nanorods: effect of reducing agent on reaction rate control", *Bull. Korean Chem. Soc*., **44**, 648 (2023).
12. E. Lukianova-Hleb, Y. Hu, L. Latterini, L. Tarpani, S. Lee, R. A. Drezek, J. H. Hafner, and DO Lapotko, "Plasmonic nanobubbles as transient vapor nanobubbles generated around plasmonic nanoparticles", *ACS Nano*, **4**, 2109 (2010).
13. K. M. Mayer, S. Lee, H. Liao, B. C. Rostro, A. Fuentes, P. T. Scully, C. L. Nehl, and J. H. Hafner, "A label-free immunoassay based upon localized surface plasmon resonance of gold nanorods", *ACS Nano*, **2**, 687 (2008).
14. K. M. Mayer, F. Hao, S. Lee, P. Nordlander, and J. H. Hafner, "A single molecule immunoassay by localized surface plasmon resonance", *Nanotechnology*, **21**, 255503 (2010).
15. W. K. Rhim, M. Kim, K. L. Hartman, K. W. Kang, and J. M. Nam, "Radionuclide-labeled nanostructures for in vivo imaging of cancer", *Nano Converg.*, **2**, 10 (2015).
16. L. Kim, S. Jo, G. J. Kim, K. H. Kim, S. E. Seo, E. Ryu, C. J. Shin, Y. K. Kim, J. W. Choi, and O. S. Kwon, "Recombinant protein embedded liposome on gold nanoparticle based on LSPR method to detect Corona virus", *Nano Converg*., **10**, 51 (2023).
17. H. Kim, S. Yoo, S. Kim, H. S. Lee, T. J. Lee, and S. Lee, "Colorimetric detection and automatic quantitative analysis of mercury(II) ions via selective redox reaction sites on silver-coated gold nanorods", *Sens. Actuators Rep*., **9**, 100256 (2025).
18. S. Lee, K. M. Mayer, and J. H. Hafner, "Improved localized surface plasmon resonance immunoassay with gold bipyramid substrates", *Anal. Chem*., **81**, 4450 (2009).
19. B. C. Rostro-Kohanloo, L. R. Bickford, C. M. Payne, E. S. Day, L. J. E. Anderson, M. Zhong, S. Lee, K. M. Mayer, T. Zal, L. Adam, C. P. N. Dinney, R. A. Drezek, J. L. West, and J. H. Hafner, "The stabilization and targeting of surfactant-synthesized gold nanorods", *Nanotechnology*, **20**, 434005 (2009).
20. S. Lee, L. J. E. Anderson, C. M. Payne, and J. H. Hafner, "Structural transition in the surfactant layer that surrounds gold nanorods as observed by analytical surface-enhanced Raman spectroscopy", *Langmuir*, **27**, 14748 (2011).
21. G. W. Park, J. W. Ko, and W. B. Ko, "Synthesis of gold nanoparticles using fullerene oxide and their catalytic activity for reduction of 4-nitroaniline", *Elast. Compos*., **54**, 105 (2019).
22. J. Watt and B. G. Hance, "Effect of seed age on gold nanorod formation: a microfluidic, real-time investigation", *Chem. Mater.*, **27**, 6442 (2015).
23. L. L. Lazarus, A. S. J. Yang, and S. Ch, "Flow-focused synthesis of monodisperse gold nanoparticles using ionic liquids on a microfluidic platform", *Lab Chip*, **10**, 3377 (2010).
24. E. Podlesnaia, P. Gerald Inangha, J. Vesenka, M. Seyring, H. J. Hempel, M. Rettenmayr, A Csáki, and W Fritzsche, "Microfluidic-generated seeds for gold nanotriangle synthesis in three or two steps", *Small*, **19**, 2204810 (2023).
25. S. Lee, P. Kumar, Y. Hu, G. J. Cheng, and J. Irudayaraj, "Graphene laminated gold bipyramids as sensitive detection platforms for antibiotic molecules", *Chem. Commun.*, **51**, 15494 (2015).
26. S. Lee, "Characterization of surface manipulation of gold nanorod with self-assembled monolayers", *J. Nanosci. Nanotechnol*., **16**, 6450 (2016).
27. S. M. Lee, D. H. Nam, D. Lee, S. H. Lim, S. J. Son, and S Lee, "Gold nanoparticles deposited on a conical anodic aluminum oxide substrate for improved surface-enhanced Raman scattering", *ACS Appl. Nano Mater*., **4**, 12905 (2021).
28. J. Kim, S. Hwang, Q. S. Luu, D. Jo, U. T. Do, Q. T. Nguyen, J. S. Kwon, S. Lee, and Y. Lee, "Development of porous silicon-coated gold nanoparticles as potential theragnostic material", *Bull. Korean Chem. Soc*., **42**, 1706 (2021).
29. S. Lee, M. G. Hahm, R. Vajtai, D. P. Hashim, T. Thurakitseree, A. C. Chipara, P. M. Ajayan, and J. H. Hafner, "Utilizing 3D SERS active volumes in aligned carbon nanotube scaffold substrates", *Adv. Mater.*, **24**, 5261 (2012).
30. S. Yoo, J. Park, D. H. Nam, S. Kim, D. Jeong, M. K. Lee, and S. Lee, "Highly sensitive SERS-active substrate with uniform gold nanostructures on heat-treated Ni foam for detection of cardiovascular disease biomarker", *Nanoscale Adv.*, **7**, 2171 (2025).
31. D. H. Nam, J. Park, S. Yoo, S. Kim, H. Kim, J. Zeng, G. Leem, and S. Lee, "Recent progress on plasmonic hybrid SERS-active substrates for molecular detection", *Appl. Spectrosc. Rev.*, 1 (2025).
32. Y. S. Yeo, J. Park, S. Yoo, D. H. Nam, H. Kim, T. J. Lee, G. Leem, J. S. Kwon, and S. Lee, "Well-defined assembly

of plasmonic metal nanoparticles by dielectrophoresis for highly sensitive SERS-active substrates", *Lab Chip*, (2025).
33. J. Fang, S. Du, S. Lebedkin, Z. Li, R. Kruk, M. Kappes, and H. Hahn, "Gold mesostructures with tailored surface topography and their self-assembly arrays for surface-enhanced Raman spectroscopy", *Nano Lett*., **10**, 5006 (2010).
34. Y. M. Lee, S. E. Kim, and J. E. Park, "Strong coupling in plasmonic metal nanoparticles", *Nano Converg*., **10**, 34 (2023).
35. A. Haryanto and C. W. Lee, "Shell-isolated nanoparticle-enhanced Raman spectroscopy for mechanistic investigation of electrochemical reactions", *Nano Converg.*, **9**, 9 (2022).
36. S. Wu, X. Zhou, X. Yang, Z. Hou, Y. Shi, L. Zhong, Q. Jiang, and Q. Zhang, "A rapid green strategy for the synthesis of Au meatball-like nanoparticles using green tea for SERS applications", *J. Nanopart. Res*., **16**, 2325 (2014).
37. S. Kim, S. Yoo, D. H. Nam, H. Kim, J. H. Hafner, and S. Lee, "Monodispersed mesoscopic star-shaped gold particles via silver-ion-assisted multidirectional growth for highly sensitive SERS-active substrates", *Nano Converg.*, **11**, 26 (2024).
38. J. Fang, S. Du, S. Lebedkin, Z. Li, R. Kruk, M. Kappes, and H. Hahn, "Gold mesostructures with tailored surface topography and their self-assembly arrays for surface-enhanced Raman spectroscopy", *Nano Lett.*, **10**, 5006 (2010).
39. H. Wang and N. J. Halas, "Mesoscopic Au meatball particles", *Adv. Mater.*, **20**, 820 (2008).
40. A. Ghosh, M. Panneerselvam, S. Mondal, P. Das, T. Singha, S. Rana, L. T. Costa, B. Satpati, S. Das, U. K. Sur, and D. Senapati, "Parallel plate capacitor model at the nanoscale for stable and gigantic SERS activity of the 4-MBA@R-AuNP–4-MBA@R-AuNP system", *ACS Omega*, **9**, 41504 (2024).
41. C. U. Wang, Y. Arai, I. Kim, W. Jang, S. Lee, J. H. Hafner, E. Jeoung, D. Jung, and Y. Kwon, "Surface-modified gold nanorods for specific cell targeting", *J. Korean Phys. Soc*., **60**, 1700 (2012).
42. S. Balamurugan, K. M. Mayer, S. Lee, S. A. Soper, J. H. Hafner, and D. A. Spivak, "Nanostructure shape effects on response of plasmonic aptamer sensors", *J. Mol. Recognit*., **26**, 402 (2013).
43. S. H. Kim, C. Lee, G. J. Jang, S. Yoo, S. Lee, S. Y. Han, "Understanding the biomolecular coronas of high-density lipoproteins on PEGylated Au nanoparticles: implication for lipid corona formation in the blood", *ACS Appl. Nano Mater.*, **5**, 2018 (2022).
44. Y. Wu, Q. Yu, Y. Joung, C. S. Jeon, S. Lee, S. H. Pyun, S. W. Joo, L. Chen, and J. Choo, "Highly uniform self-assembly of gold nanoparticles by butanol-induced dehydration and its SERS applications in SARS-CoV-2 detection", *Anal. Chem.*, **95**, 12710 (2023).